AGU PUBLICATIONS

JGR

Journal of Geophysical Research: Biogeosciences

RESEARCH ARTICLE
10.1002/2015JG003311

Key Points:
- Climate and physical forcing mechanisms influence the interannual variability of seasonal nutrient dynamics
- N or P drawdown during December-March is influenced by the Southern Annular Mode-driven sea ice and wind dynamics
- Si drawdown during November-December is influenced by early sea ice retreat

Supporting Information:
- Supporting Information S1
- Figure S1

Correspondence to:
H. Kim,
hyewon@ldeo.columbia.edu

Citation:
Kim, H., S. C. Doney, R. A. Iannuzzi, M. P. Meredith, D. G. Martinson, and H. W. Ducklow (2016), Climate forcing for dynamics of dissolved inorganic nutrients at Palmer Station, Antarctica: An interdecadal (1993–2013) analysis, *J. Geophys. Res. Biogeosci.*, *121*, 2369–2389, doi:10.1002/2015JG003311.

Received 22 DEC 2015
Accepted 19 AUG 2016
Accepted article online 26 AUG 2016
Published online 17 SEP 2016

Climate forcing for dynamics of dissolved inorganic nutrients at Palmer Station, Antarctica: An interdecadal (1993–2013) analysis

Hyewon Kim[1,2], Scott C. Doney[3], Richard A. Iannuzzi[4], Michael P. Meredith[5], Douglas G. Martinson[1,4], and Hugh W. Ducklow[1,2]

[1]Department of Earth and Environmental Sciences, Columbia University, New York, New York, USA, [2]Division of Biology and Paleo Environment, Lamont-Doherty Earth Observatory, Columbia University, Palisades, New York, USA, [3]Department of Marine Chemistry and Geochemistry, Woods Hole Oceanographic Institution, Woods Hole, Massachusetts, USA, [4]Division of Ocean and Climate Physics, Lamont-Doherty Earth Observatory, Columbia University, Palisades, New York, USA, [5]British Antarctic Survey, Cambridge, UK

Abstract We analyzed 20 years (1993–2013) of observations of dissolved inorganic macronutrients (nitrate, N; phosphate, P; and silicate, Si) and chlorophyll *a* (Chl) at Palmer Station, Antarctica (64.8°S, 64.1°W) to elucidate how large-scale climate and local physical forcing affect the interannual variability in the seasonal phytoplankton bloom and associated drawdown of nutrients. The leading modes of nutrients (N, P, and Si empirical orthogonal functions 1, EOF1) represent overall negative anomalies throughout growing seasons, showing a mixed signal of variability in the initial levels and drawdown thereafter (low-frequency dynamics). The second most common seasonal patterns of nitrate and phosphate (N and P EOF2) capture prolonged drawdown events during December–March, which are correlated to Chl EOF1. Si EOF2 captures a drawdown event during November–December, which is correlated to Chl EOF2. These different drawdown patterns are shaped by different sets of physical and climate forcing mechanisms. N and P drawdown events during December–March are influenced by the winter and spring Southern Annular Mode (SAM) phase, where nutrient utilization is enhanced in a stabilized upper water column as a consequence of SAM-driven winter sea ice and spring wind dynamics. Si drawdown during November–December is influenced by early sea ice retreat, where ice breakup may induce abrupt water column stratification and a subsequent diatom bloom or release of diatom cells from within the sea ice. Our findings underscore that seasonal nutrient dynamics in the coastal WAP are coupled to large-scale climate forcing and related physics, understanding of which may enable improved projections of biogeochemical responses to climate change.

1. Introduction

The Western Antarctic Peninsula (WAP) has responded dramatically to climate change and ocean warming in recent decades, at rates as fast or faster than any other region in the Southern Hemisphere [*Vaughan et al.*, 2003; *Schofield et al.*, 2010; *Ducklow et al.*, 2012]. The WAP is also subjected to strong interannual and seasonal variability in upper ocean dynamics and exhibits related responses in marine ecology and biogeochemistry [*Ducklow et al.*, 2006; *Ross et al.*, 2008; *Smith et al.*, 2008; *Vernet et al.*, 2008]. The Palmer Long-Term Ecological Research (PAL-LTER) project now spans over 20 years of observations (1991–2015), with a special focus on the coupling between sea ice and upper water column dynamics and related ecological processes. Interannual variability in WAP physical and biological properties is linked to two large-scale climate modes: the Southern Annular Mode (SAM) and the El Niño–Southern Oscillation (ENSO) [*Saba et al.*, 2014]. Teleconnection of the ENSO and its interactions with an inherent extratropical mode, the SAM, have been widely reported for the WAP [*Yuan and Martinson*, 2000; *Yuan*, 2004; *Hall and Visbeck*, 2002; *Marshall et al.*, 2004; *Stammerjohn et al.*, 2008]. During El Niño events, the subtropical jet strengthens and the polar frontal jet weakens, causing fewer storms and colder air temperatures and thus favorable conditions for sea ice growth in the southern Bellingshausen Sea [*Stammerjohn et al.*, 2008]. Under negative SAM (−SAM) conditions, cold southerly winds blow toward the WAP region, which also creates favorable sea ice conditions (e.g., late retreat and early advance) [*Stammerjohn et al.*, 2008]. The converse scenarios apply to both La Niña and +SAM events.

Biologically, the coastal region of the WAP is a very productive ecosystem in the Southern Ocean during the short summer growth season when light levels are high enough to support intense photosynthesis and rapid

phytoplankton growth [*Smith et al*., 1996, 1998; *Clarke et al*., 2008; *Vernet et al*., 2008; *Schloss et al*., 2012; *Ducklow et al*., 2013]. The coastal and continental shelf waters of the WAP frequently experience intense seasonal phytoplankton blooms dominated by diatoms, cryptophytes, mixed flagellates, prasinophytes, and haptophytes [*Prézelin et al*., 2000; *Garibotti et al*., 2003; *Smith et al*., 2008]. Blooms are primarily initiated by the availability of light when the upper mixed layer shoals and permits phytoplankton cells to overcome light limitation [*Mitchell et al*., 1991; *Venables et al*., 2013]. Shoaling of the upper mixed layer is influenced by seasonal sea ice dynamics, as the meltwater from sea ice results in increased stratification of the water column [*Smith et al*., 1998]. In turn, sea ice dynamics are affected by the combination of different modes of the SAM and ENSO, in addition to stochastic forcing across a range of time scales [*Stammerjohn et al*., 2008]. This atmospheric-sea ice-biomass coupling is an important mechanism determining the bloom dynamics in the WAP region. *Saba et al*. [2014] showed that positive anomalies of phytoplankton blooms every 4–6 years corresponded to the negative phase of the SAM during the preceding winter, as the −SAM promotes winter sea ice, reduces wind speeds in spring, and results in stronger water column stratification [*Venables et al*., 2013].

Although the ecological responses to physical forcing (e.g., blooms) are increasingly well understood, less is known about the interannual variability and physical controls on biogeochemical processes [*Schloss et al*., 2012]. For example, in the WAP and adjacent regions, seasonal nutrient dynamics have been the focus of several studies [*Rubin et al*., 1998; *Serebrennikova and Fanning*, 2004; *Serebrennikova et al*., 2008; *Pedulli et al*., 2014] but interannual variations in nutrient dynamics are comparatively less well understood. Phytoplankton blooms may result in complete utilization of macronutrients [*Ducklow et al*., 2012], owing to an absence of micronutrient limitation in the coastal waters of the WAP [*Smith et al*., 1996; *Serebrennikova and Fanning*, 2004]. More commonly, macronutrients are not fully depleted. Dissolved nitrate and phosphate (N and P) are gradually, but not completely, utilized during the blooms, and dissolved silicate (Si) is only utilized when diatoms dominate the blooms [*Clarke et al*., 2008]. The seasonal dynamics are broadly similar to lower latitude blooms, but their long-term variations have not been addressed.

To explore atmospheric-sea ice-biogeochemical coupling, we examined the full seasonal (October–March) dynamics of phytoplankton blooms and drawdown of dissolved inorganic macronutrients (N, P, and Si) at Palmer Station over the past 20 years (1993–2013). Using the 20 year long PAL time series, we aim to address the interannual variability in the seasonal patterns of phytoplankton blooms and dissolved inorganic macronutrients. Then, physical and climate forcing mechanisms responsible for the observed interannual variability are investigated. This analysis may serve as a valuable baseline to determine if and how phytoplankton and nutrient supply are responding to regional climate warming and sea ice loss [*Smith et al*., 2008; *Montes-Hugo et al*., 2009]. Our study extends the analysis of average summer (December–February) conditions by *Saba et al*. [2014] to biogeochemical (nutrient) processes and generalizes it to the full (October to March) growing season at semimonthly resolution.

2. Materials and Methods

2.1. Study Area

The study area is located at Palmer Station (64.8°S, 64.1°W) on Anvers Island in the Western Antarctic Peninsula (WAP). Samples were collected from a long-term monitoring station, Palmer Station B (Figure 1). Station B is relatively shallow (~75 m) and located inshore 1 km from the Marr Glacier.

2.2. Sampling and Analysis

Samples for chlorophyll *a* (Chl) and dissolved inorganic nutrients were collected at Palmer Station B on a twice-weekly basis during the growing season (October–March) in 1993–2013 with Go-Flo bottle casts from a Zodiac boat. Samples were drawn and stored for the subsequent determination of the ratio of stable isotopes of oxygen in seawater ($\delta^{18}O$); these were collected weekly in the near surface (5–10 m) starting in 2012. Nutrients analyzed for our study are nitrate plus nitrite ($NO_3^- + NO_2^-$, hereafter called nitrate due to the very low concentration of nitrite), phosphate (PO_4^{3-}), and silicate ($Si(OH)_4^-$). Sampling was commenced as soon as ice conditions permitted access by Zodiac, but sampling gaps occurred especially during the first few years, due to sea ice, bad weather, deployment changes, and other logistical reasons. No data are available for the 1996–1997, 2007–2008, and 2008–2009 field seasons for nutrients. For Chl

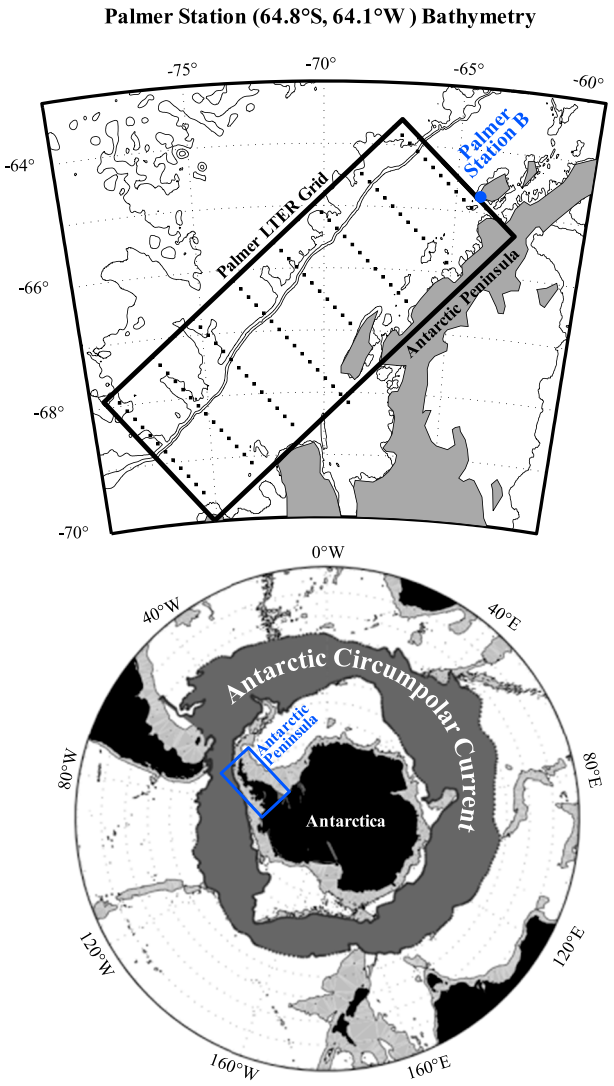

Figure 1. Map of the study area (Palmer Station B) in the west of the Antarctic Peninsula.

measurements, seawater samples were filtered onto GF/F filters and frozen at −80°C prior to fluorometric analysis [*Parsons et al*., 1984]. After storage, samples were analyzed with recognized standard oceanographic protocols for nutrient autonalyzers (i.e., continuous flow analyzers) [*Parsons et al*., 1984]. $\delta^{18}O$ measurements were performed by stable isotope mass spectrometry, with full details (including uncertainties) presented in *Meredith et al*. [2008]. The time series data for Chl (Data set 126, doi:10.6073/pasta/012de0cf7d1f00951-b7289037a3a4c19) and nutrients (Data set 211, are available at the Palmer LTER Datazoo at http://oceaninformatics.ucsd.edu/datazoo/data/pallter/dataset.

2.3. Standing Stock Calculations

Depth-integrated standing stocks (mg m^{-2} for Chl and mmol m^{-2} for nutrients) were calculated by integrating concentrations from the surface to 50 m, the average depth at which nutrients first reflected maximum water column concentrations for the site. It was not always possible to discern a physically meaningful boundary such as the depth of temperature minimum or maximum (T_{min} or T_{max}) due to the shallow water column depths, whereas 50 m provided a consistent basis of comparison across months, seasons, and years. Further details are given in Text S1 in the supporting information.

2.4. Climate Variability

We used two different climate indices (Table 1) to assess the atmospheric teleconnections to the study region: The Southern Annular Mode (SAM) and the Multivariate El Niño–Southern Oscillation (ENSO) Index (MEI). The monthly SAM index for the 1993–2013 period was obtained from the British Antarctic Survey (http://www.nerc-bas.ac.uk/icd/gjma/sam.html). The monthly MEI was obtained from the NOAA Earth System Research Laboratory (http://www.esrl.noaa.gov/psd/data/correlation/mei.data).

2.5. Sea Ice Parameters

Sea ice data were obtained from passive microwave satellite imagery in the PAL region (daily sea ice concentration surrounding PAL hydrostation 600.040, 20 km from Palmer Station B; Table 1). Five annual sea ice indices were examined: day of advance, day of retreat, ice days, ice persistence, and total sea ice cover [*Stammerjohn et al*., 2008]. Day of advance is the day when sea ice cover first exceeded 15% and stayed above that threshold for at least five consecutive days. Day of retreat is the last day when sea ice cover remained above the 15% threshold for five consecutive days. Ice days are the number of days between day of advance and day of retreat, whereas ice persistence is an actual number of days in which sea ice cover was above 15%. Total sea ice cover was additionally calculated as the sum of sea ice cover (%) in a given sea ice year (i.e., 1 March of a given year to 28 February of the next year). Monthly areal sea ice coverage for the

Table 1. Summary of Climate and Physical Oceanographic and Biogeochemical Variables Used in the Study[a]

Category	Variable	Definition
Climate indices	MEI	Monthly Multivariate El Niño–Southern Oscillation (ENSO) Index
	SAM	Monthly Southern Annular Mode (SAM) index
Meteorology	Wind speed ($m\,s^{-1}$)	Daily averaged time series of wind speed measured by manual observations and PALMOS automatic weather station measurements
	Air temperature (°C)	Daily averaged time series of air temperature measured by manual observations and PALMOS automatic weather station measurements
	SST (°C)	Daily averaged time series of sea surface temperature measured by manual observations and PALMOS automatic weather station measurements
Sea ice indices	Annual indices; day of advance (day)	The first day when sea ice cover first exceeded 15% and stayed above the threshold for at least five consecutive days
	Annual indices; day of retreat (day)	The last day when sea ice cover remained above the 15% threshold for five consecutive days
	Annual indices; ice days (days)	The number of days between day of advance and day of retreat
	Annual indices; ice persistence (days)	An actual number of days in which sea ice cover was above 15%
	Annual indices; total ice cover (% days)	The sum of sea ice cover in a given sea ice year (i.e., 1 March of a given year to 28 February of the next year)
	Monthly indices; sea ice extent (km^2)	Total surface area within the ice edge
	Monthly indices; sea ice area (km^2)	Actual area of sea ice covered ocean inside ice edge based on satellite-derived sea ice concentration (e.g., including area of openings and leads within the ice edge)
Water column stability parameters	$Depth_{T\min}$ (m)	Depth of temperature minimum; the layer of the remnant cold Winter Water (WW) from the previous winter
	SD_s (m)	Summer salt deficit, calculated as the amount of autumn sea ice required to develop in order to eliminate the seasonal halocline or the amount of excess freshwater from the surface to the seasonal halocline relative to that of WW
	$\Delta\sigma_{\theta\text{-}T\min}$ ($kg\,m^{-3}\,m^{-1}$)	Salinity-driven density gradient, calculated as the density difference between the surface layer and the layer of $T_{\min}$ divided by the depth difference between the two
	MLD (m)	Seasonal mixed layer depth, calculated as the deepest point of physically mixed layer of water from the surface
Biogeochemical variables	Chl standing stock ($mg\,m^{-2}$)	Depth-integrated (to 50 m) amount of volumetric chlorophyll *a* values ($\mu g\,L^{-1}$)
	N standing stock ($mmol\,m^{-2}$)	Depth-integrated (to 50 m) amount of volumetric $NO_3^- + NO_2^-$ values ($\mu mol\,L^{-1}$)
	P standing stock ($mmol\,m^{-2}$)	Depth-integrated (to 50 m) amount of volumetric PO_4^{3-} values ($\mu mol\,L^{-1}$)
	Si standing stock ($mmol\,m^{-2}$)	Depth-integrated (to 50 m) amount of volumetric $Si(OH)_4^-$ values ($\mu mol\,L^{-1}$)

[a]The list shows indices of climate, meteorology, sea ice, water column stability, and biogeochemical stocks.

greater PAL region (Data set 34 at Palmer LTER Datazoo, doi:10.6073/pasta/a69864292c4499-ee5587d53491796ff2; Figure 1 and Table 1) was also examined: sea ice extent (km^2) and area (km^2). Sea ice extent indicates the total surface area inside the ice edge, while sea ice area is the area of sea ice-covered ocean inside the ice edge based on satellite-derived sea ice concentrations.

2.6. Water Column Stability Parameters

To investigate local water column stratification parameters, physical oceanographic data (including temperature, conductivity, and pressure) were collected for the study period using various instruments (i.e., a SeaBird Electronics Seacat SBE 19 from 1991 to 2007, a SeaBird Electronics Seacat SBE 19 plus from 2006 onward, and a Falmouth Scientific Inc. FSI MCTD-3 and a Satlantic HyperPro-II from 2008 on). We used four different water column stability parameters during November–December as indices of conditions favorable for spring and summer phytoplankton blooms (Table 1): depth of temperature minimum ($depth_{T\min}$), seasonal mixed layer depth (MLD), summer salt deficit in the upper 25 m (SD_s), and salinity-driven density gradient from surface to $depth_{T\min}$ ($\Delta\sigma_{\theta\text{-}T\min}$). Further details for calculating these indices are available in *Martinson and Iannuzzi* [1998]. The $depth_{T\min}$ (m) indicates the layer of the remnant cold Winter Water (WW) from the previous winter. The MLD (m) is defined as the deepest point of homogeneously mixed layer of water from the surface based on vertical profiles of σ_θ. The SD_s (m) is defined as the amount of autumn sea ice required to eliminate the seasonal halocline or the amount of excess freshwater from the surface to the seasonal halocline relative to that of WW (more details in *Martinson et al.* [2008]). The $\Delta\sigma_{\theta\text{-}T\min}$ ($kg\,m^{-3}\,m^{-1}$) is calculated as the density difference between the surface layer and the layer of $T_{\min}$ divided by the depth difference between the two.

Table 2. Nutrient Drawdown Statistics[a]

	N		P		Si	
Year	Drawdown (mmol m^{-2})	Period of Drawdown (Days of Year)	Drawdown (mmol m^{-2})	Period of Drawdown (Days of Year)	Drawdown (mmol m^{-2})	Period of Drawdown (Days of Year)
1993	349	290–365 (75 days)	21	290–365 (75 days)	1620	305–365 (60 days)
1994	415	290–395 (105 days)	22	320–395 (75 days)	758	350–440 (90 days)
1995	533	290–395 (105 days)	15	290–380 (90 days)	1387	305–395 (90 days)
1997	300	290–440 (150 days)	15	290–380 (90 days)	1260	305–410 (105 days)
1998	307	290–380 (90 days)	19	290–410 (120 days)	710	290–440 (150 days)
1999	337	305–365 (60 days)	19	290–380 (90 days)	1006	305–380 (75 days)
2000	509	305–365 (60 days)	26	320–365 (45 days)	1170	305–380 (75 days)
2001	541	290–395 (105 days)	43	320–395 (75 days)	1520	320–380 (60 days)
2002	531	290–440 (150 days)	16	290–380 (90 days)	613	305–425 (120 days)
2003	352	305–380 (75 days)	12	290–365 (75 days)	648	305–440 (135 days)
2004	209	290–395 (105 days)	24	305–380 (75 days)	899	305–380 (75 days)
2005	507	290–380 (90 days)	37	290–380 (90 days)	618	305–395 (90 days)
2006	339	290–395 (105 days)	37	305–410 (105 days)	1303	290–395 (105 days)
2009	558	290–380 (90 days)	29	290–365 (75 days)	834	305–395 (90 days)
2010	441	305–395 (90 days)	9	290–380 (90 days)	1340	290–440 (150 days)
2011	358	290–350 (60 days)	17	320–365 (45 days)	468	320–440 (120 days)
2012	319	290–335 (45 days)	12	290–320 (30 days)	403	305–440 (135 days)
2013	571	290–380 (90 days)	36	290–380 (90 days)	1090	305–395 (105 days)
Mean	Drawdown amount: 415 ± 110 mmol m^{-2} Drawdown window: 293 ± 6 − 385 ± 26 days of year (92 ± 28 days)		Drawdown amount: 23 ± 10 mmol m^{-2} Drawdown window: 298 ± 13 − 378 ± 20 days of year (79 ± 23 days)		Drawdown amount: 985 ± 368 mmol m^{-2} Drawdown window: 307 ± 14 − 408 ± 27 days of year (100 ± 29 days)	

[a]The table shows the net amount of seasonal drawdown and periods of the apparent drawdown events of each standing stock for each study year. Drawdown amounts and periods were estimated as described in the text.

2.7. Meteorology

Daily weather has been recorded (air temperature, pressure, wind speed, wind direction, precipitation, and sky cover) at Palmer Station by both manual observations and an automated system since April 1989. Data were obtained from the Palmer meteorology database (Data set 28 at Palmer LTER Datazoo, doi:10.6073/pasta/50627a6eb69afce74859b8349d9f8dc4; Table 1).

2.8. Empirical Orthogonal Function (EOF) Decomposition

We employed EOF decomposition to investigate statistically coherent patterns and fill in the gaps in the Chl and nutrient standing stock data sets using reduced space optimal analysis (RSOA) [*Kaplan et al*., 1997]. A detailed discussion of the EOF analysis is given in Text S2.

2.9. Nutrient Drawdown Statistics

Plots of the RSOA-interpolated Chl and nutrients for each year were visually inspected to track a seasonal-scale increase (decrease) in the Chl (nutrient) standing stock that represents seasonal phytoplankton blooms (bloom-driven drawdown of nutrients). The seasonal changes in the Chl (nutrient) standing stocks were calculated as the difference between the initial minimum (maximum) and the later seasonal maximum (minimum) standing stocks (Table 2). The mean initial maximum values prior to drawdown events are 1428 ± 77, 91 ± 10, and 3979 ± 274 mmol m^{-2} for N, P, and Si, respectively. This change represents the net annual drawdown (net removal) for each nutrient, and the amplitude (intensity) of the bloom, if any occurred.

2.10. Correlating Standing Stock PCs to Climate and WAP Physical Variables

To explore relationships between the standing stock PCs and potential forcing climate and physical variables responsible for the EOF patterns, we correlated the annual PCs to climate indices (SAM and ENSO), sea ice (sea ice extent and area), water column stability (bulk stability), and biogeochemical indices (Chl and nutrients). To fix autocorrelation-induced inflation in the sample size (i.e., autocorrelation in the PCs of the decomposed Chl and nutrient data sets), we employed the bootstrap technique. Additional details for the bootstrap method are given in Text S3.

Table 3. Summary of Fundamental End-Member Water Types, Tracer Values, and Weights Used in Optimal Multiparameter Analysis (OMP)[a]

	End-Member Property Values (*A*)			
Tracer	CDW	SIM	MET	Weights (*w*)
S	34.65	7	0	20
$\delta^{18}O$ (‰)	0	1.1	−12	20
Si^* ($\mu mol\,L^{-1}$)	54.07	5.9	0	0.1237

[a]Three end-member water property (salinity (S), $\delta^{18}O$, and Si^*) values for different source water types (CDW, SIM, and MET), their uncertainties, and original sources of values are listed. See Text S4 for details. S_{CDW}: calculated from 1998 to 2008 climatology of CDW in the LTER Slope stations. S_{SIM}: *Meredith et al.* [2013]. S_{MET}: *Meredith et al.* [2013]. $\delta^{18}O_{CDW}$: *Meredith et al.* [2013]. $\delta^{18}O_{SIM}$: *Meredith et al.* [2013]. $\delta^{18}O_{MET}$: *Meredith et al.* [2013]. Si^*_{CDW}: calculated from 1998 to 2008 climatology of CDW in the LTER Slope stations. Si^*_{SIM}: *Fransson et al.* [2011]. Si^*_{MET}: *Rysgaard et al.* [2012].

2.11. Optimal Multiparameter Analysis

The observed nutrient stocks and their variability are due to some unknown combination of biological (uptake and regeneration) and physical (mixing and advection) processes. To compute nutrient concentrations expected by purely physical processes (i.e., effects of biological drawdown excluded) and to demonstrate the dilution effects on nutrients by freshwater inputs, Optimal Multiparameter (OMP) analysis was employed [e.g., *Martinson et al.*, 2008]. Similar to *Tomczak and Large* [1989], but not normalizing the property matrix in our case, OMP analysis enables quantification of the mixing ratios or relative fractions of *n* different source water types at a point location using *m* different conservative (e.g., S and $\delta^{18}O$) or quasi-conservative tracer properties (e.g., nutrient tracers; $Si^* = [SiO_4] - [NO_3]$). The fundamental source water types in our study include sea ice meltwater (SIM), meteoric (glacial and precipitation inputs) water (MET), and Circumpolar Deep Water (CDW) as an oceanic source. CDW was chosen as the oceanic end-member, instead of WW, allowing for the fact that the freshening effect from glacial and sea ice includes the level of freshening needed to convert the WAP variant of CDW to WW and is consistent with the WAP being a region of relatively weak net advection compared with the Antarctic Circumpolar Current or the subpolar gyres [*Meredith et al.*, 2008, 2013]. We used three different end-member water properties (tracers), salinity (S), $\delta^{18}O$, and Si^* at Palmer Station B. End-member tracer values and weights used in the analysis are found in Table 3 with their origins. Phosphate concentrations from the three source water types are $P_{CDW} = 2.22$ (σ of $P_{CDW} = 0.44$, calculated from 1998 to 2008 climatology of CDW in the LTER Slope stations), $P_{SIM} = 0.26$ (σ of $P_{SIM} = 0.43$) [*Fransson et al.*, 2011], and $P_{MET} = 0.00$ (σ of P_{MET} not available) [*Rysgaard et al.*, 2012]. Details of the mathematical solutions for OMP analysis are described in Text S4.

3. Results

3.1. Atmospheric-Sea Ice-Biogeochemical Coupling by Monthly and Annual Averages

To explore potential connections from climate variability to biogeochemistry in the system, linear regressions were performed among climate, sea ice, water column stability, phytoplankton bloom, and nutrient variables (i.e., monthly and annual averages of the raw data for sea ice variables and monthly averages for the rest of the variables).

Overall, there was a clear connection between each group of dynamics: climate variability to sea ice dynamics, sea ice to upper water column physics, water column dynamics to phytoplankton bloom, and bloom to nutrients (Figure 2). Both SAM and ENSO were significant predictors of sea ice variability (Figures 2a–2c). Notably, the impacts of SAM on sea ice were opposite between winter and spring. Negative SAM during winter (August) results in large sea ice area (Figure 2a), while positive SAM during spring (September) promotes total ice cover (Figure 2b). Similar to the winter SAM effect on sea ice, winter El Niño (i.e., positive MEI) predicts more sea ice extent in the following spring with a lag of 4 months (Figure 2c). Increased sea ice conditions (i.e., ice extent, ice persistence, and day of retreat) always result in stratification of the upper water column via high SD_s (Figures 2d–2f). In turn, the more stabilized water column (i.e., shallow MLD) was correlated with large phytoplankton accumulations but with weak correlations. Shallow November–December averaged MLD leads to high Chl with lags of 1–2 months (Figures 2g and 2h).

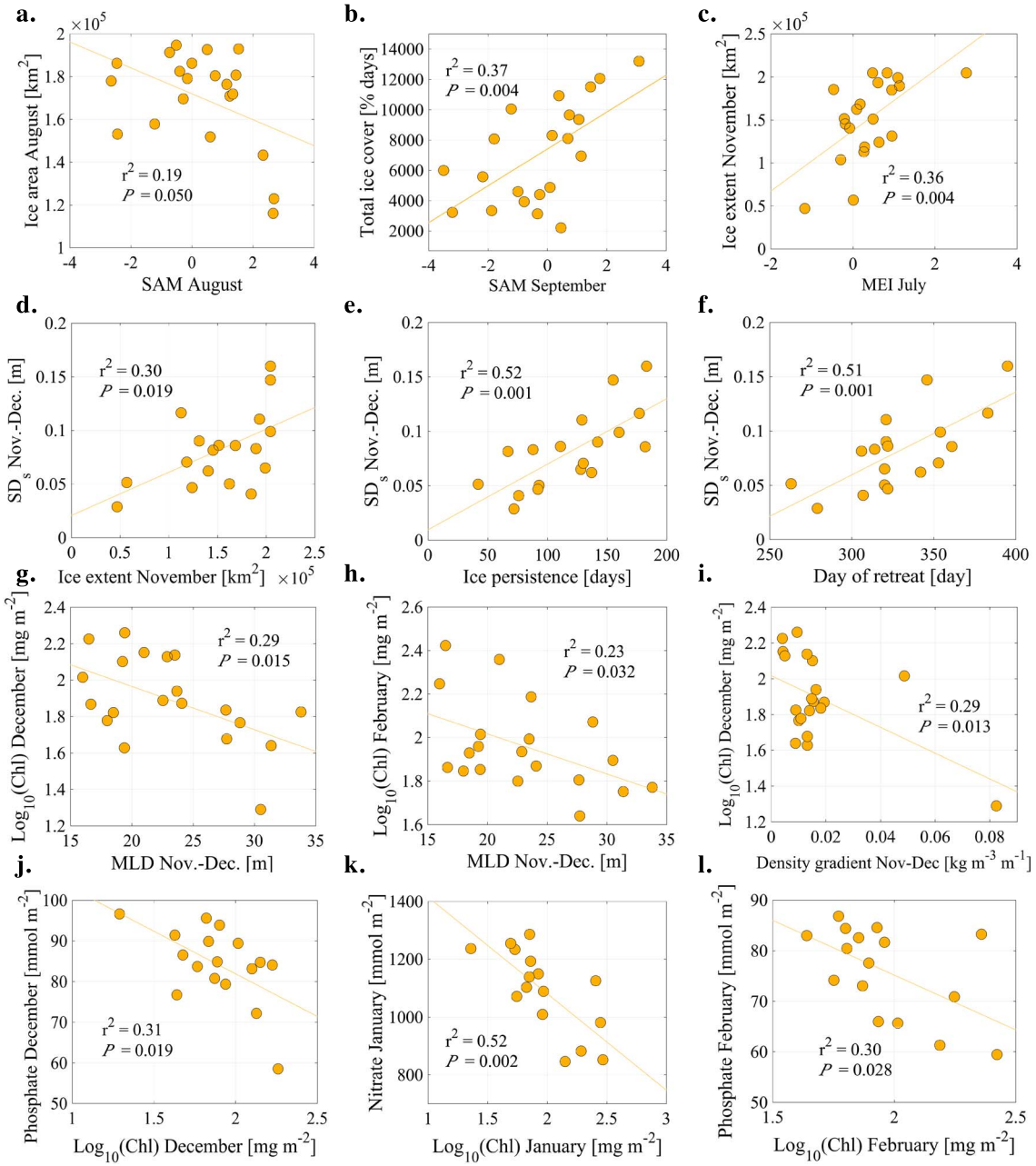

Figure 2. Linear regressions among climate and local physical oceanographic and biogeochemical variables. Statistically significant results are presented here among all correlations performed. (a–c) Climate variability versus sea ice variables. (d–f) Sea ice variables versus water column stability parameters. (g–i) Water column stability parameters versus monthly chlorophyll (Chl). (j–l) Monthly Chl versus monthly mean of nutrient standing stock.

However, high $\Delta\sigma_{\theta\text{-}T\min}$ results in low Chl, showing a conflicting result (Figure 2i). The increased Chl was significantly correlated with decreased standing stocks of both phosphate (Figures 2j and 2l) and nitrate (Figure 2k), indicative of biological drawdown of macronutrients by phytoplankton utilization.

3.2. Climatology of Seasonal Nutrient Dynamics

When the standing stocks are averaged for each time window over the 20 year (1993–2013) period, there are clear climatological seasonal progressions from mid-October to end-March for the three nutrients and Chl (Figure 3). A gradual buildup in Chl from the start of our sampling period indicates the development of a sustained bloom, which peaks at 118 mg m^{-2} in January–February (Figure 3a). By the end of March, Chl

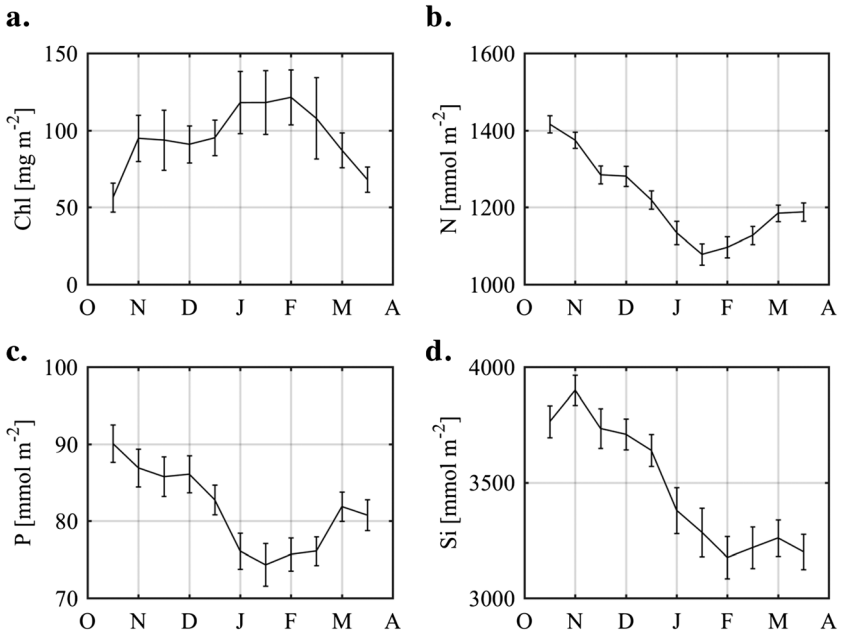

Figure 3. Climatology plots of depth-integrated Chl and nutrients. Climatology (1993–2013) of depth-integrated (0–50 m) (a) Chl, (b) N, (c) P, and (d) Si standing stock values for a full growing season (October to March) with error bars indicating 1 standard error. Samples were binned into 15 day intervals. The data included in the calculation are interpolated using RSOA (see text for details).

has nearly returned to its starting (prebloom) value. The nutrient stocks show the complimentary pattern of a seasonal drawdown from a winter maximum to a minimum in January–March (Figures 3b–3d).

The seasonal maximum of N (1416 mmol m^{-2}) in mid-October is depleted by ~24%, reaching a seasonal minimum of 1078 mmol m^{-2} in mid-January (i.e., a drawdown of 338 mmol N m^{-2}; Figure 3b). After this apparent seasonal drawdown, N returns to 81% of its starting (predrawdown) maximum value by the end of our observations in early fall. The P standing stock shows a similar pattern of seasonal depletion; the seasonal minimum at 74 mmol m^{-2} in mid-January is a result of ~21% drawdown of the seasonal maximum of 90 mmol m^{-2} in mid-October (Figure 3c). Approximately 88% of the maximum P standing stock has been recovered by the end of season. The similarity in drawdown and recovery suggests strong coupling between N and P utilization in a climatological sense. The seasonal minimum values of N and P are observed at the same time as the peak Chl in January. Seasonal drawdown of the Si standing stock results in a 23% decrease of the standing stock, with its maximum at 3900 mmol m^{-2} in the beginning of November and the minimum of 3176 mmol m^{-2} in the beginning of February (Figure 3d). However, Si does not show evidence of returning to its original level, at least during our observation period. Thus, the consistency of N, P, and Si utilization patterns (not the recovery patterns) suggests a strong influence of diatom growth on the overall climatology. On average (from climatology) N:P drawdown ratio is ~21, Si:N drawdown ratio is 2.1, N:P recovery ratio is 12.8, and Si:N recovery ratio is 3.1.

3.3. Interannual Variability of Seasonal Nutrient Dynamics

The climatologies mask great interannual and intraseasonal variability. Comparison with individual years (Figures 4–7) shows that this climatology is the result of averaging many individual blooms occurring at various times, with varying duration, in different years. With a few exceptions, most individual years do not closely resemble the climatologies.

Based on the EOF and PC patterns of the Chl and nutrient anomalies relative to the climatologies, this section focuses on seasonal variability patterns for Chl and nutrients (i.e., EOF, Table 4) and how these seasonal patterns vary interannually (i.e., PC). The first and second EOFs (EOFs 1–2, Figures 8a, 8c, 8e, and 8g) represent the first two dominant, uncorrelated, and independent seasonal variability patterns. Annual standing stock

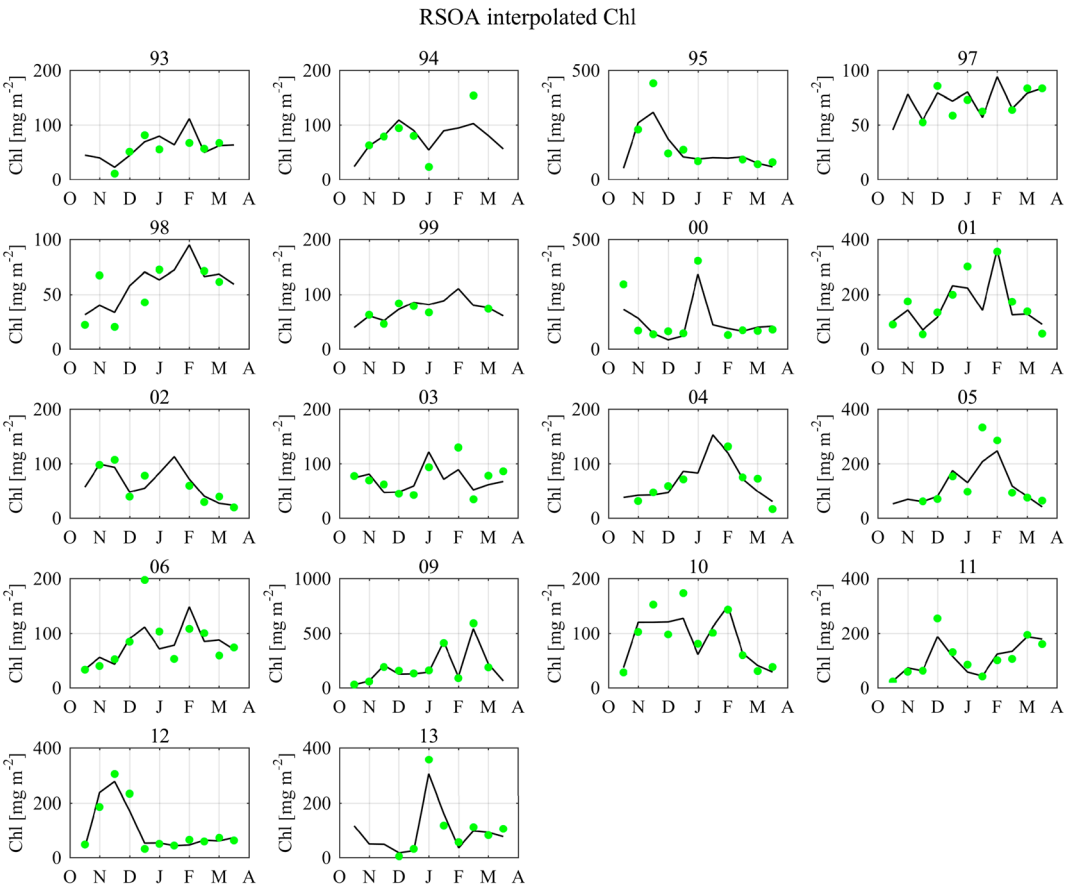

Figure 4. Reduced space optimal analysis (RSOA) interpolated (black solid line) seasonal time series of Chl for each year, overlaid with 15 day mean values of raw data points (dots) prior to the interpolation. Year annotations indicate the starting year of the Austral growing season (i.e., 93 is for October 1993 to March 1994).

anomalies (Figures 8b, 8d, 8f, and 8h) reconstructed from the first five leading modes show the combined effects of the different seasonal patterns on each year of observation. The first two EOF modes explained 46–77% of the total variability.

Chl mode 1 (26% of total Chl variability) reveals that the most common seasonal pattern is driven by an extended phytoplankton bloom, from early December to the end of March, with a peak in March and a secondary peak in December–January (Figure 8a, EOF1). This extended December-to-March bloom or "DJFM bloom" occurs every 4–6 years as shown by the PC (Figure 9a, PC1; years 1995, 2001, 2005, 2009, and 2011). To compare high DJFM bloom years from the PC, we calculated an index for a high bloom year from the anomaly plots by averaging anomalies of each seasonal time window throughout each year (i.e., average anomaly index). The DJFM bloom year based on the PC was accordingly seen as a high bloom year (i.e., a positive value of the average anomaly index) in the anomaly plots (average anomaly index = 0.34 for 1995, 0.57 for 2001, 0.20 for 2005, and 0.52 for 2009 in Figure 8b). This is the dominant signal in the Chl variability. Chl mode 2 (20% of total Chl variability) represented a late spring bloom with a peak in early December (Figure 8 a, EOF2). This November-to-December (ND) bloom or spring bloom pattern was indicated by large PC values (Figure 9a, PC2) and seen in the anomaly plots (1995, 2000, 2010, and 2012; Figures 8b and 9a). Strictly speaking, the ND spring bloom is not uncommon, but neither is it a perennial feature.

The EOF patterns for nutrients appear to be more complex compared to those of Chl. Unlike the gradual, seasonal increase of Chl in the lowest mode (Chl EOF1), modes 1 of P and Si captured rather flat (i.e., a single negative sign of anomaly with little fluctuation in the values) and seasonally consistent, overall low nutrient levels throughout the entire growth season. Mode 1 of N also captured an initial lack of nutrient in the very beginning of the season and then prolonged negative anomalies, which is briefly interrupted by a positive

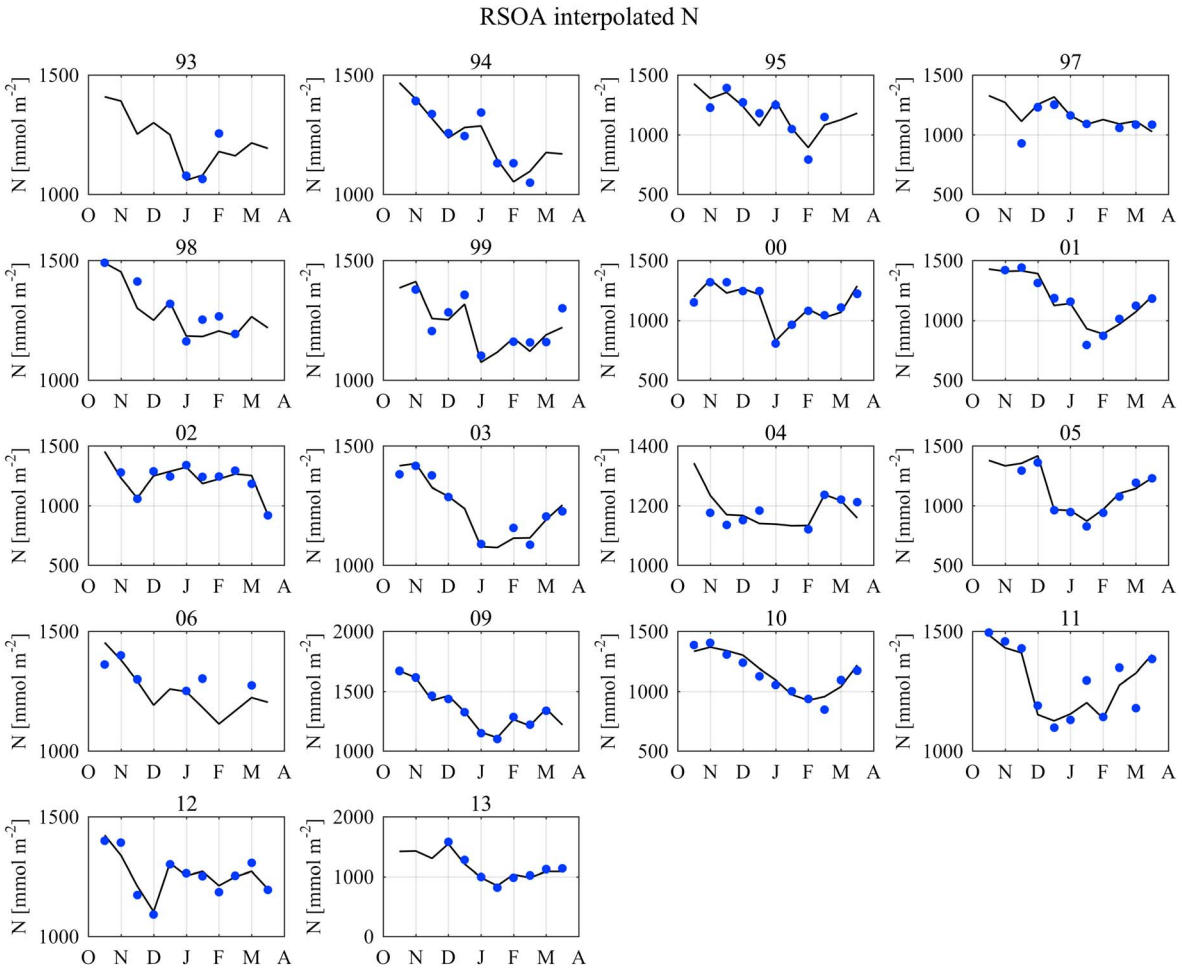

Figure 5. RSOA-interpolated (black solid line) seasonal time series of N for each year, overlaid with 15 day mean values of raw data points (dots) prior to the interpolation.

anomaly in December. Due to the low nutrients prior to the bloom development, modes 1 of all three nutrients are far from simply indicating seasonal drawdown. Instead, they represent a mixed signal of both a drop in the baseline of the initial, prebloom nutrient standing stocks and seasonal drawdown as a result of the bloom. There were no statistically significant correlations in the interannual variability of the DJFM bloom and modes 1 (i.e., overall negative anomalies) of all three nutrients (all $P > 0.05$ for Chl PC1 versus N, P, and Si PC1).

In contrast, modes 2 of N and P captured season-long drawdown starting from mid-December, which also corresponds well to the window of the overall bloom (Figures 8a, 8c, and 8e). Indeed, there were significant correlations in the interannual variability of the DJFM bloom (i.e., Chl) and the DJFM drawdown of N and P, which are indicative of biological drawdown of both N and P ($r = 0.67$, $P = 0.0022$ for Chl PC1 versus N PC2 and $r = 0.49$, $P = 0.0414$ for Chl PC1 versus P PC2). Mode 2 of Si is characterized by a negative peak (a negative anomaly relative to the climatology) during mid-November to mid-December. This November–December drawdown of Si corresponds to the peak of the ND spring bloom with a significant correlation ($r = 0.67$, $P = 0.0023$ for Chl PC2 versus Si PC2), indicating utilization of Si by diatom-dominated assemblages in the spring bloom.

In summary, EOF decomposition of Chl and nutrients shows a varying seasonal phenology, variable intensity of the processes (bloom and nutrient drawdown), and perhaps varying controls of winter low-frequency dynamics in terms of initializing the nutrient standing stocks and their interactions in a complex manner.

3.4. Physical and Climate Forcing Mechanisms for Nutrient Dynamics

To identify the most important forcing mechanisms for the nutrient dynamics, we first established significant correlations among climate, sea ice, and water column stability parameters (Figure 10, a-e). A La Niña

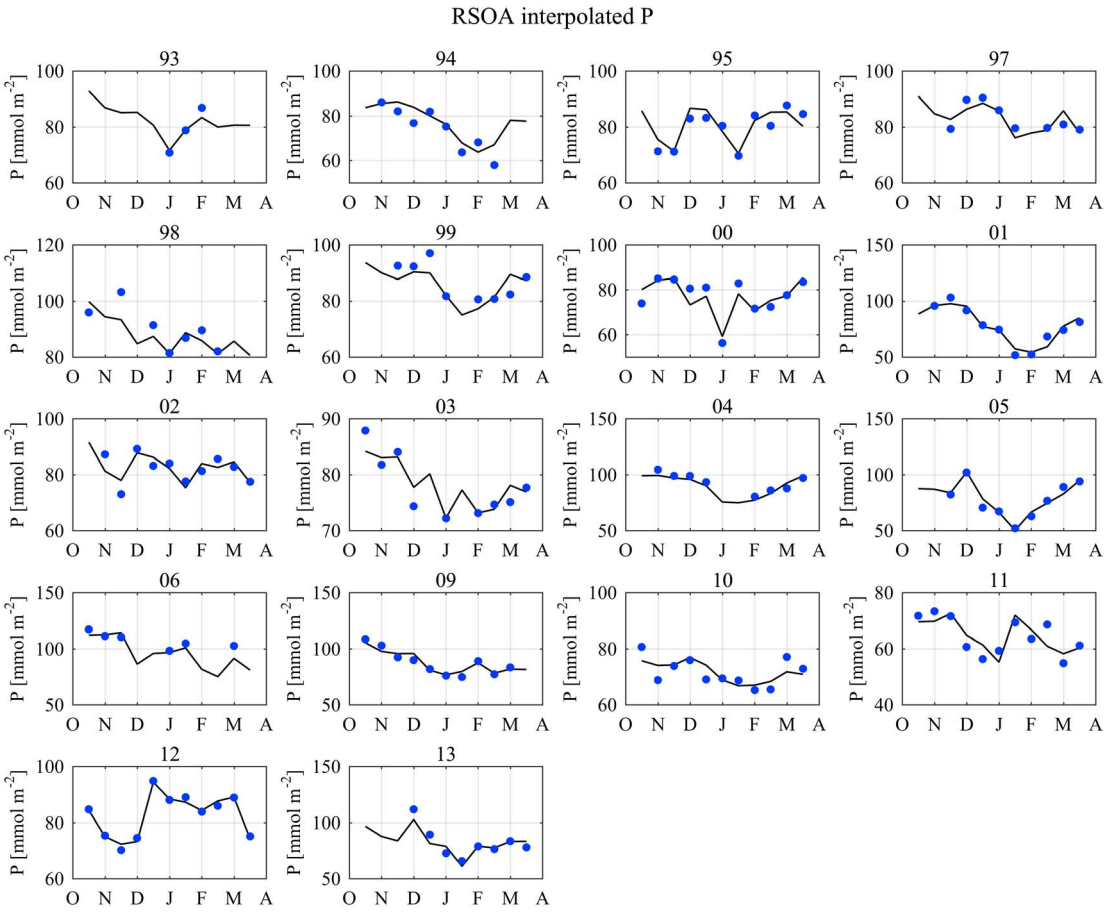

Figure 6. RSOA-interpolated (black solid line) seasonal time series of P for each year, overlaid with 15 day mean values of raw data points (dots) prior to the interpolation.

condition (i.e., negative MEI) in the preceding winter (August) resulted in less sea ice extent in the following spring (October) (Figure 10, a), while negative SAM in the preceding winter (July) created a high winter sea ice (July) extent (Figure 10, b). A positive phase of spring (October) SAM caused high spring wind speeds (Figure 10, d). As a result of seasonal ice melt, high winter (July) sea ice extent promoted stratification of the upper water column via increased SD_s (Figure 10, c). In contrast, intense wind conditions in spring (December) significantly disrupted the stability of the water column via decreased $\Delta\sigma$-$\theta_{T\min}$ (Figure 10, e).

Next, we performed cross correlations between the Chl PCs and climate/physical variables to examine the climate-nutrient link given the significant correlations established between the PCs of Chl and nutrients (section 3.3). The two common seasonal patterns of nutrients were predicted by different scenarios of physical and climate setup events. For the DJFM drawdown of N and P (N and P PC2) by the DJFM bloom (Chl PC1), significant physical predictors were a shallow MLD (Figure 10, f-h), negative winter (July) SAM ($r = -0.46$, $P = 0.031$), and positive spring (October) SAM ($r = 0.39$, $P = 0.071$). Thus, a scenario for the DJFM drawdown of N and P was composed of two distinct sets of forcings or pathways: "winter SAM pathway" (Figure 10, b-c-f-h) and "spring SAM pathway" (Figure 10, d-e-f-h). The opposite phases of the winter and spring SAM cause contrasting effects on stability of the upper water column, where −SAM in the winter enhances stratification while +SAM in the spring leads to weaker stratification. However, both contribute to initiation and termination of the bloom in a concerted manner (see discussion section 4.4).

Conversely, a significant physical predictor for the ND drawdown of Si (Si PC2) by the ND (diatom) bloom (Chl PC2) was a decreased spring (October) sea ice extent (Figure 10, g-i). Thus, a scenario for the ND drawdown of Si was a spring sea ice pathway (Figure 10, a-g-i). Although significant correlations were absent with Chl PC2, this drawdown also tended to occur under La Niña in preceding winter (data not shown).

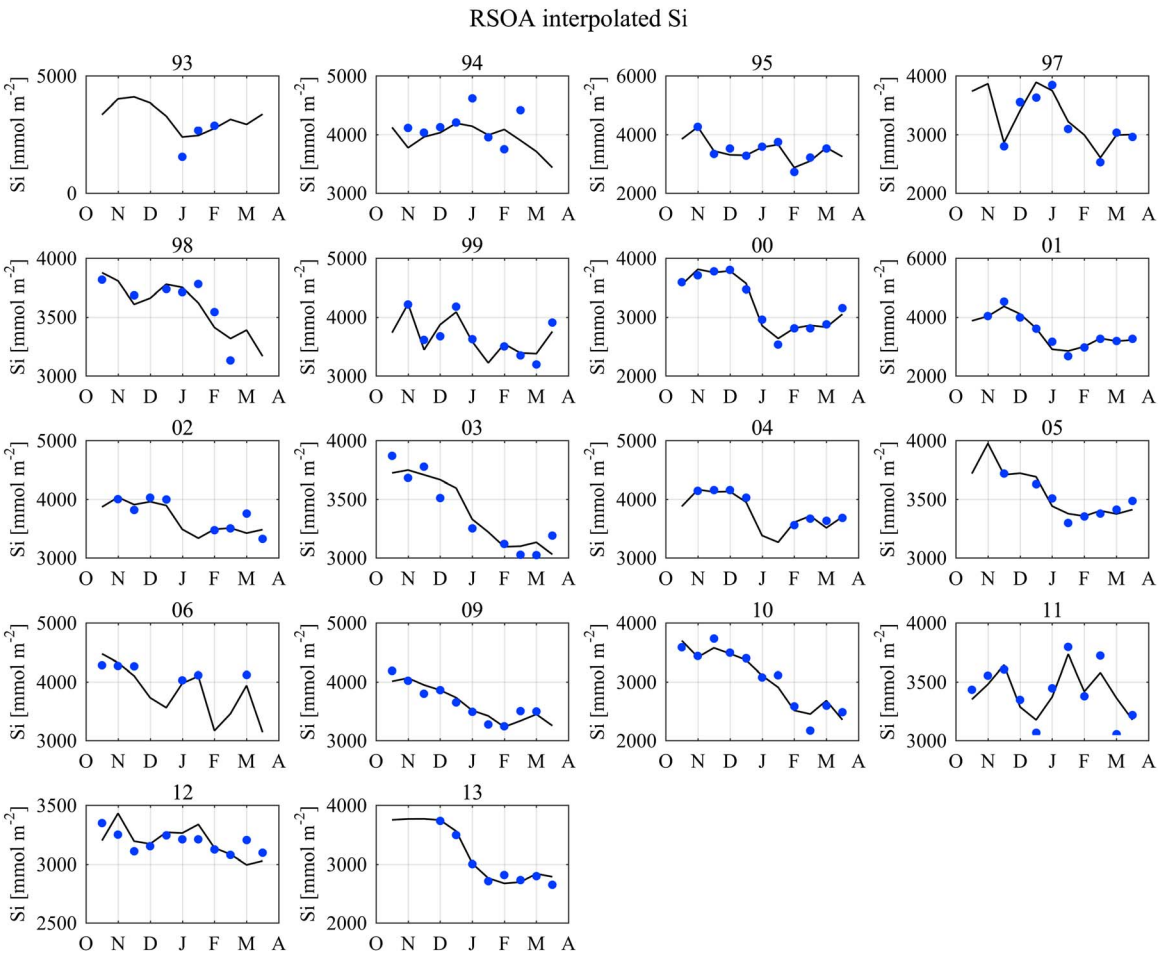

Figure 7. RSOA-interpolated (black solid line) seasonal time series of Si for each year, overlaid with 15 day mean values of raw data points (dots) prior to the interpolation.

3.5. Dilution Effect by Sea Ice and Meteoric Water

We used an OMP analysis (see Text S4 for details) to evaluate the contributions to observed nutrient stocks from physical (as compared to biological) sources: additions from high nutrient CDW and dilution by freshwater (SIM and MET) inputs. First-order estimates are provided by examples from 2011 to 2012 and 2012 to 2013, the first years for which we have $\delta^{18}O$ tracer data. In years 2011–2012, the water mass composition for the surface layer was characterized with 95.2–97.1% CDW, 0–1.3% SIM, and 1.9–4.0% MET (Table 5). Thus, we mainly focused on the freshening effect by MET due to relatively minimal fractions of SIM compared with MET. As fractions of MET increase from the beginning of the season and peak in mid-January, P concentration decreases correspondingly by 0.04 μmol L^{-1} from the maximum 2.16 μmol L^{-1} to the minimum 2.12 μmol L^{-1} due to dilution (Table 5). P concentrations increase again to ~76% of the early season maximum as the relative fraction of MET declines after mid-January. In years 2012–2013, fractions of MET were more dominant (1.6–4.3% of water composition) than SIM (0–0.6%) (Table 5).

The dilution effect on P by MET in years 2012–2013 was also similar to previous years, but with no evidence of recovery of the P concentration as season progressed. P declined by 0.06 μmol L^{-1} from its seasonal maximum of 2.19 μmol L^{-1} in mid-December to the minimum of 2.13 μmol L^{-1} at the end of the season as the MET fraction kept increasing (Table S1). This freshwater input-driven dilution of P in the water column (0.04 μmol L^{-1} and 0.06 μmol L^{-1} for years 2011–2012 and 2012–2013, respectively) was, however, still within the ranges of uncertainties of P for both years; mean S.D. of P = 0.48 μmol L^{-1} and mean S.D. of P = 0.47 μmol L^{-1} for years 2011–2012 and 2012–2013, respectively (Table S1). Therefore, OMP analysis

Table 4. Summary of Seasonal Patterns Captured by EOF for Depth-Integrated Chl and Nutrients[a]

	Seasonal Patterns Captured by EOF	
Variable	EOF1 (PC1)	EOF2 (PC2)
Log_{10}(Chl)	Extended summer (DJFM) bloom (26%)	Spring (ND) bloom (20%)
N	Overall negative anomalies (37%)	DJFM drawdown of nitrate (26%)
P	Overall negative anomalies (56%)	DJFM drawdown of phosphate (22%)
Si	Overall negative anomalies (58%)	ND drawdown of silicate (19%)

[a]Seasonal patterns of blooms and associated nutrient drawdown for depth-integrated nitrate, phosphate, and silicate as captured by the first two EOFs (see Figure 8). Their interannual variability is presented as PC time series (see Figure 9). Percent number in parentheses indicates a fraction of variability explained by each EOF among total standing stock variability.

showed (1) that nutrients were not significantly diluted by meltwater from glacial runoff and precipitation in the recent 2 years and (2) that nutrients need to be diluted at least an order of magnitude more (to overcome the range of errors of 0.47–0.48 μmol L^{-1} if generalized to further years), as a result of increased inputs of MET or SIM, to distinguish meltwater-driven decrease of nutrients from the effects of biological drawdown.

4. Discussion

Various studies have demonstrated that the coastal WAP is a very productive ecosystem with strong seasonal and interannual variability of phytoplankton blooms and primary productivity [*Moline et al*., 2001; *Vernet et al*., 2008; *Smith et al*., 2008; *Saba et al*., 2014]. The bloom variability in the system is largely modulated by stratification of the upper water column as a consequence both of winter sea ice growth and spring sea ice melt, which are in turn influenced by large-scale ENSO and SAM variability [*Stammerjohn et al*., 2008]. In the coastal WAP, observations indicate that macronutrients are sufficiently abundant to support large phytoplankton biomass accumulations; accordingly, it is possible that (biology-driven) nutrient variability closely resembles bloom variability and may also be influenced by similar physical forcing. Besides a few studies on nutrient dynamics [*Rubin et al*., 1998; *Serebrennikova and Fanning* 2004; *Serebrennikova et al*., 2008; *Pedulli et al*., 2014; *Hauri et al*., 2015], long-term nutrient dynamics, especially in terms of seasonal and interannual variability, still remain poorly understood. Here using an interdecadal data set (1993–2013) of nutrients over the entire austral growth season (October–March), we decompose seasonal patterns of each macronutrient (N, P, and Si), demonstrate how each pattern's annual variations (i.e., interannual variability) covary with bloom variability, and discuss their physical and climate drivers. We also address physically driven variability (e.g., glacial melt) in the nutrients. This study spans temporally the longest and best resolved record of nutrient variability in Antarctic waters and will help in understanding the responses of other biogeochemical processes to both climate variability and climate change along the WAP.

4.1. Atmospheric-Sea Ice-Biogeochemical Coupling by Monthly and Annual Averages

To first order, our results from linear regression of raw data values (Figure 2) showed that there was a clear link between each group of dynamics (i.e., climate, sea ice, water column stability, bloom, and nutrients), implying an ultimate control of climate on nutrient variability. However, simply using monthly composites of variables may not be sufficient to capture meaningful fluctuations or variability (i.e., events and processes) on submonthly to monthly time scales. This is also evidenced by contradictory results seen between water column stability and the magnitude of blooms. Strong interannual variability in the magnitude and timing of bloom events also complicates analysis of the patterns. Thus, more detailed analysis of nutrient and bloom phenology was performed to decompose independent (orthogonal) seasonal patterns first and to examine their changes over time to understand interannual variability in the seasonal characteristics.

4.2. Climatology of Seasonal Nutrient Dynamics

Individual years showed a strong variability in the timing, duration, frequency, and intensity of phytoplankton blooms and nutrient drawdown and recovery patterns, consistent with high seasonal and interannual variability of physical, ecological, and biogeochemical processes typically observed in Antarctic coastal waters (Figures 4–7). The climatologies reflect a composite of several bloom events with different timing, duration, and magnitude in different years, rather than showing an unchanging annual bloom pattern. In the blooms we observed over 1992 to present, only $<$30% of macronutrients were utilized. This implies that macronutrients were sufficient to support large phytoplankton accumulations and were not limiting factors in the WAP

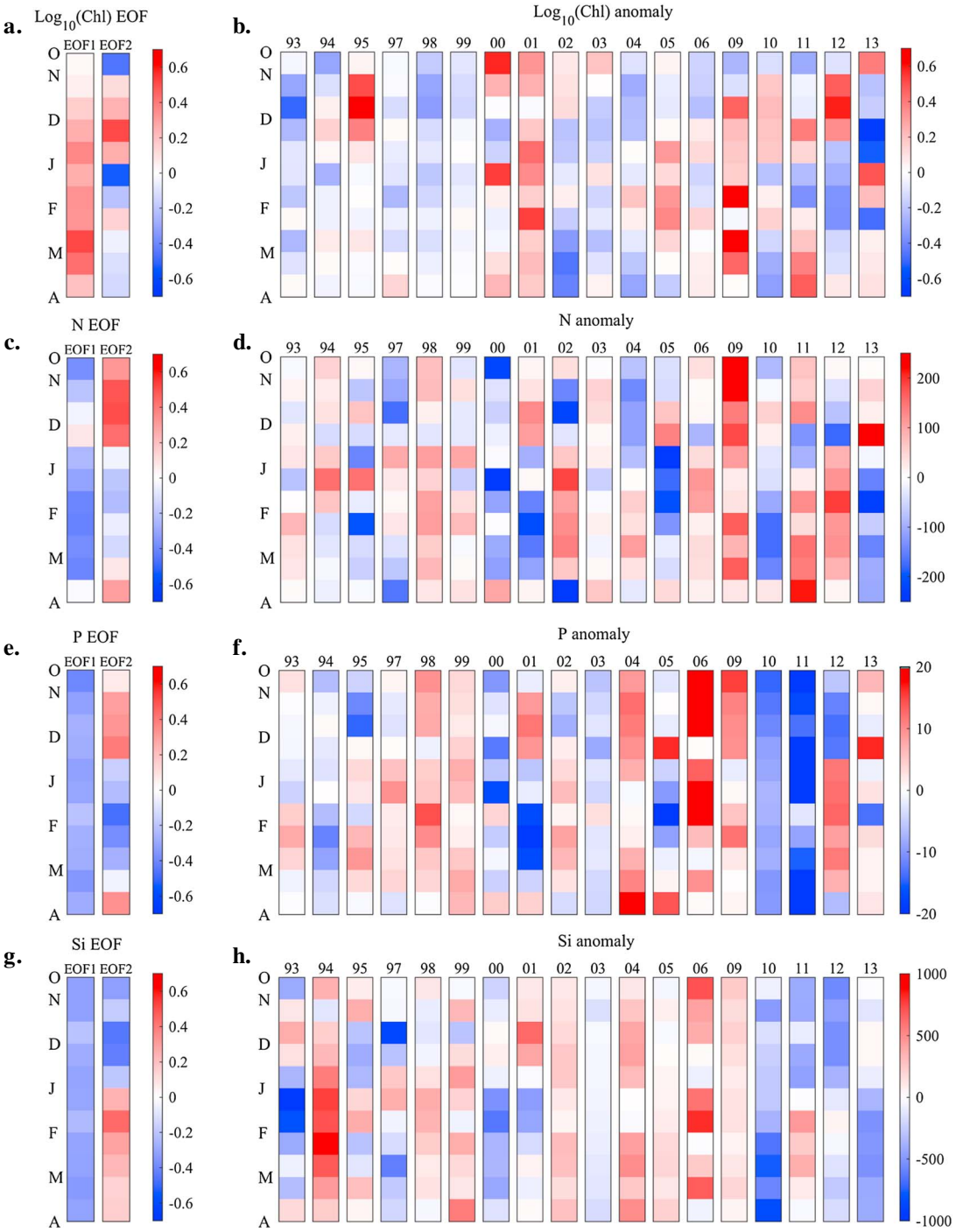

Figure 8. Empirical orthogonal function (EOF) and anomaly plots of depth-integrated Chl and nutrients. The (a, c, e, and g) EOF patterns and (b, d, f, and h) anomaly plots reconstructed using the first five dominant EOF modes comprising 85–90% of the variability. Higher modes were considered noise and ignored. Scientific interpretations of the EOF patterns are summarized in Table 4. The percentage explained by each mode is represented in the corresponding principal component (PC) time series (Figure 9). The red colors represent positive anomalies, and the blue colors represent negative anomalies (relative to the climatology) in the color bars. Year annotations indicate the starting year of the Austral growing season (i.e., 93 is for October 1993 to March 1994). Note that there are year gaps in the anomaly plots (no data in 96, 07, and 08).

coastal waters [*Serebrennikova and Fanning*, 2004; *Ducklow et al.*, 2012]. This suggests that some other factors limit complete utilization of macronutrients at Palmer Station, such as irradiance or micronutrient limitation [*Saba et al.*, 2014]. The nutrient concentrations become gradually recovered as phytoplankton utilization

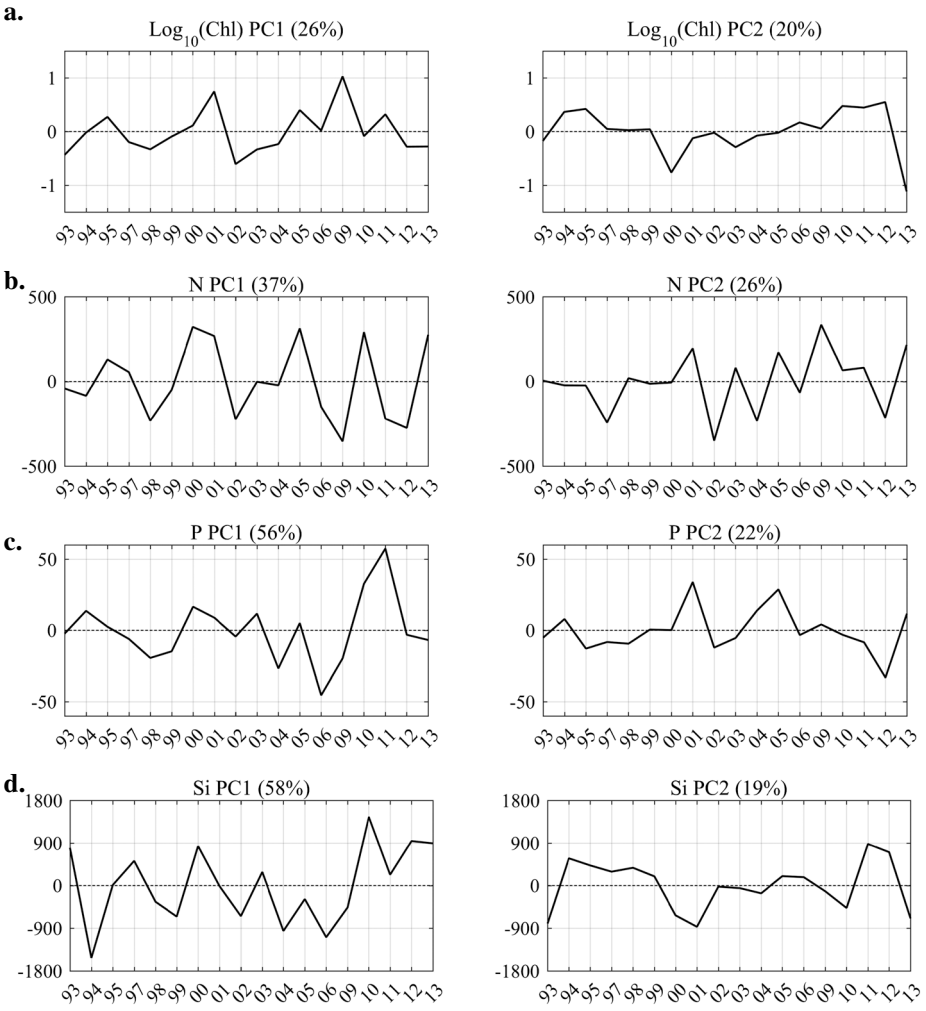

Figure 9. Principal component (PC) time series of depth-integrated Chl and nutrients. PC time series of standing stocks indicate interannual variability of the seasonal patterns detected by corresponding EOF. (a) Chl, (b) N, (c) P, and (d) Si. Headers on plots indicate the property and amount of explained variability in PCs 1 and 2 (right and left columns). Note the year gaps in the PC time series (no data in 96, 07, and 08).

slows down from the bloom collapse (not the other way around since phytoplankton here are not macronutrient limited) as well as a result of increased vertical mixing and advection as growing seasons progress.

Previous ecological studies based on EOF analyses in the WAP region consistently presented a discrepancy in the patterns between the leading modes and the climatologies for chlorophyll, primary production, and macrozooplankton abundance [*Smith et al*., 2008; *Vernet et al*., 2008; *Ross et al*., 2008]. Similarly, in our case, the climatology of Chl is not identical to the most common seasonal pattern (Chl EOF1), with a difference in the timing of bloom peaks. The climatologies of nutrients are also notably different from the most dominant seasonal signals in the nutrients (N, P, and Si EOF1), where the climatologies show a prolonged, seasonal drawdown, but EOF1 of nutrients shows a fluctuation in the baseline of the initial standing stocks (see below section 4.3 for details). Furthermore, there is no indication for the climatology of an early season spring bloom (Chl EOF2) influencing the annual cycle.

Based on the climatologies, the Redfield N:P ratio falls between our observed N:P drawdown ratio and N:P recovery ratio. Somewhat high Si:N drawdown ratio from our study might indicate a presence of diatom cells in the bloom and/or more heavily silicified diatoms. The Si:N recovery ratio is higher than the Si:N drawdown ratio, implying a dominance of nondiatom cells near the end of growing seasons. Elevated Si:N consumption ratio of diatom cells has been shown to be associated with Fe-limited conditions, but there is no evidence of iron limitation in the Palmer Station waters.

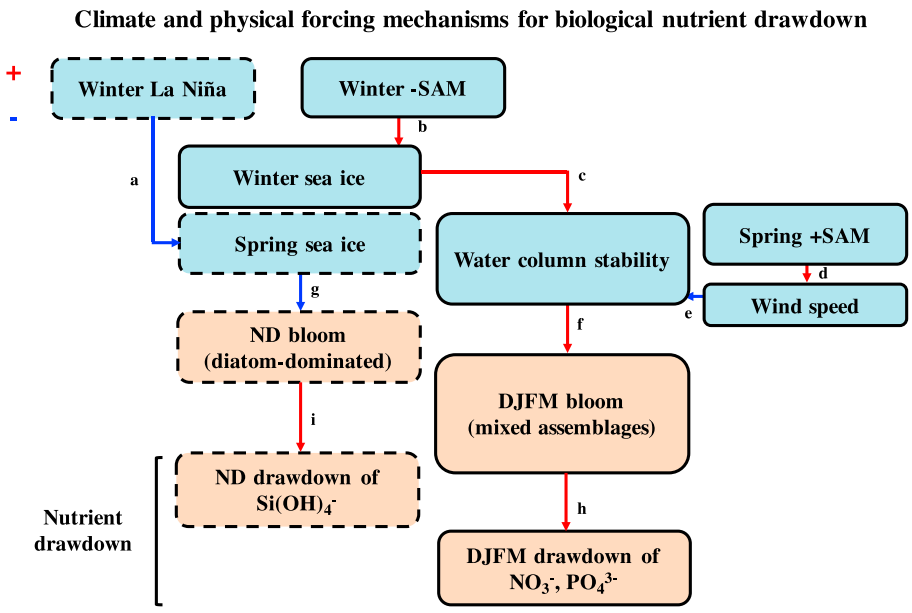

a. MEI August vs. Ice extent October (r = 0.60, P <0.001)
b. SAM July vs. Ice extent July (r = -0.30, P = 0.044)
c. Ice extent July vs. SD_s November-December (r = 0.42, P = 0.063)
d. SAM October vs. Wind speed December (r = 0.30, P = 0.069)
e. Wind speed December vs. $\Delta\sigma_{0\text{-}Tmin}$ November-December (r = -0.40, P = 0.064)
f. MLD November-December vs. Log_{10}(Chl) PC1 (r = -0.63, P = 0.001)
g. Ice extent October vs. Log_{10}(Chl) PC2 (r = -0.35, P = 0.033)
h. Log_{10}(Chl) PC1 vs. N PC2 (r = 0.67, P = 0.002)
   Log_{10}(Chl) PC1 vs. P PC2 (r = 0.49, P = 0.041)
i. Log_{10}(Chl) PC2 vs. Si PC2 (r = 0.67, P = 0.002)

Figure 10. Physical and climate forcing mechanisms of biological nutrient drawdown. Based on the observed correlations among variables, we propose two separate forcing mechanisms for different phenologies of nutrient drawdown patterns: (1) December–March (DJFM) drawdown of nitrate and phosphate and (2) November–December (ND) drawdown of silicate. Red and blue arrows indicate positive and negative effects of the top box on the box below, respectively. Extended summer (DJFM) drawdown of nitrate and phosphate is indicated by compartments with solid outlines and includes two pathways initiated by winter SAM (b-c-f-h) and spring SAM (d-e-f-h). Forcing mechanisms of late spring (ND) drawdown of silicate (i.e., diatom blooms) are represented as compartments with dotted outlines, via a spring sea ice pathway (a-g-i). Each forcing mechanism is fully explained in sections 3.4, 4.4, and 4.5. Significant regressions for each connection are given below the figure.

4.3. Interannual Variability of Seasonal Nutrient Dynamics

EOF decomposition successfully demonstrates biological drawdown of nutrients based on interactions and covariability with Chl. EOF decomposition also reveals ecologically meaningful patterns in the seasonal patterns of phytoplankton blooms, especially varying phenology, with the most dominant signal in the Chl variability (Chl EOF1) as the December to March (DJFM) bloom and the second common signal (Chl EOF2) as the spring (November–December, ND) bloom. The DJFM bloom leads to the DJFM pattern of nitrate and phosphate drawdown (N and P EOF2), while the ND bloom results in the ND drawdown of silicate (Si EOF2) by diatom-dominated assemblages in the bloom.

Conversely, the most dominant seasonal patterns in the nutrients (N, P, and Si EOF1) represent a combination of bloom-driven drawdown of nutrients and variability in the baseline of the prebloom, initial nutrient levels replenished by deep winter mixing, and convection, which in turn depend on wind stress [*Trull et al.*, 2001; *Martinson et al.*, 2008; *Ducklow et al.*, 2012]. Due to the leading modes' mixed effects, correlations with bloom variability are not always observed.

4.4. Physical and Climate Forcing for the DJFM Drawdown of Nitrate and Phosphate

Different scenarios of local physical and large-scale climate forcing mechanisms influence the phenology of blooms and nutrient drawdown based on our results from correlations between time series under each

Table 5. Summary of Relative Fractions of Different Water Types With Uncertainties (σ) and RMSE of Water Tracer Properties Between Observed and Predicted Values From OMP Analysis for the Field Season 2011–2012[a]

Field Season 2011–2012								
Day of Year	CDW (%)	SIM (%)	MET (%)	Predicted P (μmol L^{-1})	Predicted S	Predicted δ^{18}O (‰)	Predicted Si* (μmol L^{-1})	Residuals P (μmol L^{-1})
328	97.1	0.9	1.9	2.162	33.726	−0.219	52.583	0.814
358	96.2	1.1	2.8	2.141	33.395	−0.319	52.059	0.943
363	97.1	0.3	2.6	2.160	33.672	−0.304	52.530	1.012
371	96.5	0.2	3.3	2.145	33.441	−0.399	52.177	1.183
380	96.6	0.6	2.8	2.149	33.511	−0.329	52.265	1.016
388	96.6	0	3.4	2.148	33.484	−0.404	52.253	1.126
392	95.7	0.6	3.6	2.130	33.214	−0.429	51.800	1.463
399	95.5	0.5	4.0	2.124	33.116	−0.474	51.652	1.073
406	95.9	0.4	3.7	2.134	33.266	−0.434	51.892	0.983
413	95.6	1.3	3.1	2.129	33.220	−0.354	51.775	1.111
421	95.2	1.2	3.6	2.120	33.079	−0.419	51.563	0.800
427	97.1	0	2.9	2.159	33.646	−0.348	52.506	0.999
434	96.9	0	3.1	2.153	33.563	−0.376	52.377	0.920
444	96.9	0	3.1	2.154	33.569	−0.374	52.386	1.085
449	96.9	0	3.1	2.154	33.571	−0.374	52.389	1.130
455	97.0	0	3.0	2.157	33.613	−0.359	52.454	1.081
462	97.0	0	3.0	2.157	33.618	−0.357	52.462	1.185
	σ_{CDW} (%)	σ_{SIM} (%)	σ_{MET} (%)		RMSE S	RMSE δ^{18}O	RMSE Si*	RMSE P
	0.7	0.6	0.5		0.011	0.028	47.634	1.065

[a]Phosphate values predicted as a linear sum of $f_{CDW}P_{CDW} + f_{SIM}P_{SIM} + f_{MET}P_{MET}$ (see equation (6) in Text S4). The result for year 2012–2013 is available in the supporting information (Table S1).

group of dynamics. Correlations between individual pairs are used here to determine potential causal relationships; however, the statistical significance of the overall correlation chains (i.e., from climate to nutrient drawdown via sea ice or water column stability) might be difficult to determine, especially while still preserving the direction of flow in the entire chain of mechanisms. Instead, we additionally examined generalized linear models (GLMs) for drawdown of each nutrient via stepwise regression analysis. Among the GLMs for N, P, and Si drawdown, only phosphate showed that its drawdown for the DJFM period (P PC2) was expressed as a linear sum of negative winter (July) SAM, increased SD_s, and elevated DJFM bloom (high Chl PC1) simultaneously (Table S2), which is consistent with "the winter SAM pathway" (Figure 10, b-c-f-h). This might give additional confidence in assessing the robustness of our conclusions primarily based on individual pairwise correlations. Nitrate or silicate drawdown in GLMs was slightly different from the pathways in Figure 10, where only part of the hypothesized physical and climate forcing variables were observed as significant predictors for N or Si drawdown (data not shown). Importantly, no direct correlations were observed between climate (at the topmost of the mechanisms in Figure 10) and nutrient drawdown (at the very bottom of the mechanisms in Figure 10). However, there is no a priori reason to suppose that these results simply indicate no coupling between climate and nutrient variability. It suggests, rather, that the coupling is modulated through physical and ecological processes.

In the coastal waters of the WAP, diatoms and cryptophytes typically dominate large phytoplankton accumulations [*Villafañe et al.*, 1993; *Moline and Prezelin*, 1996; *Kang et al.*, 2001; *Garibotti et al.*, 2003; *Kozlowski*, 2008]. The two groups usually show a seasonal succession, with earlier dominance by diatoms in spring as sea ice retreats and later dominance by cryptophytes in warmer, fresher waters in summer as glacial ice melting further promotes water column stability through freshwater inputs [*Moline et al.*, 2001; *Garibotti et al.*, 2005; *Dierssen et al.*, 2002; *Meredith et al.*, 2013]. In a final successional stage (i.e., late summer), a mixture of diatoms and other groups again dominates the blooms [*Moline and Prezelin*, 1996; *Garibotti et al.*, 2005]. In this respect, the DJFM bloom in our study likely reflects the seasonal succession of different phytoplankton groups throughout the growing season. The presence of these different assemblages (Chl EOF1) might also preclude significant correlations with the seasonal patterns of Si (Si EOF).

Both winter and spring SAM pathways influenced the DJFM drawdown of nitrate and phosphate. Under negative SAM conditions in the preceding winter, increased winter sea ice conditions promote water

column stability via SD_s as sea ice melts, induces a diatom bloom [*Saba et al*., 2014], and thus nutrient drawdown in spring. As the growing season further progresses, under +SAM in spring, wind speeds increase, disrupting the established stability of the upper water column. This may temporally inhibit or terminate the diatom bloom, induce the replacement of diatoms by other phytoplankton groups [*Walsh et al*., 2001; *Garibotti et al*., 2005], and sustain nutrient drawdown throughout summer. This succession corresponds to the seasonal pattern for DJFM bloom (Chl EOF1) where the strong peak of a positive anomaly reappears in January–February ~1–2 months after the late December peak. In this sense, our result suggests that weaker stratification as a result of increased wind forcing leads to termination of the first stage of the seasonal blooms, and provides a chance to other taxa to bloom, resulting in a dominant pattern of sustained drawdown of nitrate and phosphate by March. The periodicity (every 4–6 years) of high DJFM bloom years in our study corresponds well with positive anomalies of mean DJF Chl reported by *Saba et al*. [2014].

4.5. Physical and Climate Forcing for the Springtime Drawdown of Silicate

Another 20% of total Chl seasonal variability represents a shorter, springtime diatom bloom as revealed by the strong correlation between Chl PC2 and Si PC2. As seen in the climatology and individual years' plots, this ND spring bloom is not a ubiquitous, annually occurring feature. Further comparisons with high-performance liquid chromatography pigment data sets (Data set 130 at Palmer LTER Datazoo, doi:10.6073/pasta/5038a45eba2f436f14e14dc5da15d090) reveal that the ND bloom years mostly corresponded to elevated diatom-specific fucoxanthin (Figure S1), suggesting that the ND drawdown of silicate is likely driven by diatoms.

In contrast to the physical mechanisms driving the DJFM drawdown of nitrate and phosphate, the ND drawdown of silicate is shaped by reduced spring sea ice extent, which usually results from La Niña conditions in the preceding winter. Lower spring sea ice extent can also be interpreted as an early spring ice retreat, as shown by a significant correlation between sea ice extent and retreat ($r = 0.56$, $P = 0.0083$ for October sea ice extent versus day of retreat). The ND Si drawdown years thus also corresponded to negative anomalies of day of sea ice retreat. We suggest two possibilities for the ND drawdown of silicate including (1) formation of diatom blooms as sea ice breaks, melts, and introduces an abrupt input of ice-derived freshwater to the surface ocean that induces strong stratification and/or (2) release of diatom cells residing within the sea ice. Both these events foster ice edge-associated spring diatom blooms [*Knox*, 2006; *Moline et al*., 2008; *Smith et al*., 2008]. However, it should be noted that this relationship is also complicated by the fact that sea ice retreat in the WAP region is often the result of wind-driven advection, rather than in situ melting [*Stammerjohn et al*., 2008].

4.6. Effects of Dilution on Nutrient Variability

In addition to biological drawdown of nutrients, physical processes may also be directly responsible for temporal fluctuations in nutrient levels. The effect of dilution by sea ice and meteoric (glacial discharge and precipitation) freshwater on nutrients was estimated by OMP analysis, where the end-member fractions corresponded well with fractions calculated by *Meredith et al*. [2013]. It is sometimes hypothesized that Palmer Station B is considerably impacted by freshwater inputs from the adjacent Marr Glacier [*McClintock et al*., 2008]. Consistent with this finding, our results show that freshwater fractions are dominated by meteoric (glacial) water, which tends to increase with seasonal warming and subsequently dilutes nutrient concentrations. The amount of dilution due to meteoric water, however, still fell within the range of uncertainties and is considered insignificant compared to biological drawdown. Assuming that sea ice melt will be still minor compared with meteoric water at our study site in future years, nutrients need to be further diluted at least an order of magnitude more to equal the range of uncertainties of 0.47–0.48 $\mu mol\,L^{-1}$, which corresponds to approximately ~16% more meteoric water than the observed maximum (in terms of a fraction contribution).

Freshwater from glacier melting poses an important question about biogeochemical processes in an era of climate change along the WAP [*Vaughan et al*., 2003; *Schofield et al*., 2010; *Ducklow et al*., 2012]. With current trends of atmospheric and ocean warming, freshwater inputs are likely increasing as a result of increasing sea ice and glacial melt in addition to increasing precipitation [e.g., *Liu et al*., 2004; *Parkinson*, 2004; *Thomas et al*., 2008; *Ducklow et al*., 2012], though it is notable that in northern Marguerite Bay, where a decade-long time series of oxygen isotope data exists, there has been a decline in meteoric water in the upper mixed layer due to increasing vertical mixing driven by sea ice loss [*Meredith et al*., 2013]. In principle, freshwater inputs dilute nutrients; even so, not every input event may cause the decrease of nutrients; rather, the impacts

depend on the phase of the bloom and nutrient drawdown at the time of the input event. The seasonal timing of blooms and nutrient drawdown may also be subject to climate change. These nonlinear aspects of biogeochemically responsive physical processes complicate understanding but will be important to explore in future to further elucidate the nutrient dynamics in this rapidly changing region.

5. Summary

In summary, our major findings are as follows.

1. Linear regressions with annual indices only provide a crude way to examine the atmospheric-sea ice-biogeochemical coupling, without demonstrating the effects of phenology and event-scale biological drawdown of nutrients.
2. Climatologies reveal a general, seasonally prolonged drawdown of all three nutrients obscuring strong seasonal and interannual variability in individual years.
3. The most dominant seasonal signals of all three nutrients (N, P, and Si EOF1) show a combination effect of variability in the baseline of initial nutrient levels prior to bloom development (presumably set by winter-time mixing dynamics) and of bloom-driven nutrient drawdown as the season progresses. These signals are not significantly correlated with bloom variability.
4. The second most common seasonal signals of nitrate and phosphate (N and P EOF2) represent summer-long DJFM drawdown as a result of the DJFM bloom (Chl EOF1), which consists of a succession of mixed phytoplankton assemblages.
5. The second most common seasonal signal of silicate (Si EOF2) represents the ND drawdown as a result of the ND bloom (Chl EOF2), dominated by diatoms.
6. Different physical and climate forcing mechanisms are responsible for the decomposed seasonal (EOF) and interannual (PC) variability of the nutrients. Years of high DJFM drawdown of nitrate and phosphate are influenced by both a winter and spring SAM pathways (Figure 10, b-c-f-h and Figure 10, d-e-f-h). In contrast, years of high ND drawdown of silicate are predicted by a spring sea ice pathway linked to La Niña (Figure 10, a-g-i).
7. The effect of freshwater (sea ice, glacial melt, and precipitation) input-driven dilution on nutrients does not appear to be significant, as examined for the case of phosphate concentration. However, if long-term climate change and ocean warming accelerate along the WAP, it is anticipated that the frequency and importance of this process could increase and subsequently further complicate an overall behavior of nutrients in the coastal waters along the WAP, along with changing biological variability.

Acknowledgments

We thank the many current and former PAL-LTER team members for their assistance with field sampling, processing, and analyzing nutrient and chlorophyll samples. Palmer LTER was supported by U.S. National Science Foundation awards OPP-9011927, 9632763, 0217282, 0823101, and GEO-PLR 1440435. H. Kim was supported as a PhD candidate by Columbia University and by a subcontract to LDEO from NASA ROSES award NNX14AL86G to S. Doney (WHOI). The data used in this manuscript can be found at the Palmer LTER Datazoo at http://oceaninformatics.ucsd.edu/datazoo/data/pallter/dataset.

References

Clarke, A., M. P. Meredith, M. I. Wallace, M. A. Brandon, and D. N. Thomas (2008), Seasonal and interannual variability in temperature, chlorophyll and macronutrients in northern Marguerite Bay, Antarctica, *Deep Sea Res., Part II*, *55*(18), 1988–2006.

Dierssen, H. M., R. C. Smith, and M. Vernet (2002), Glacial meltwater dynamics in coastal waters west of the Antarctic Peninsula, *Proc. Natl. Acad. Sci. U.S.A.*, *99*, 1790–1795.

Ducklow, H. W., W. Fraser, D. M. Karl, L. B. Quetin, R. M. Ross, R. C. Smith, S. E. Stammerjohn, M. Vernet, and R. M. Daniels (2006), Water-column processes in the West Antarctic Peninsula and the Ross Sea: Interannual variations and foodweb structure, *Deep Sea Res., Part II*, *53*(8), 834–852.

Ducklow, H. W., et al. (2012), The marine system of the Western Antarctic Peninsula, in *Antarctic Ecosystems: An Extreme Environment in a Changing World*, pp. 121–159, Blackwell, London.

Ducklow, H. W., et al. (2013), West Antarctic Peninsula: An ice-dependent coastal marine ecosystem in transition, *Oceanography*, *26*(3), 190–203.

Fransson, A., M. Chierici, P. L. Yager, and W. O. Smith Jr. (2011), Antarctic sea ice carbon dioxide system and controls, *J. Geophys. Res.*, *116*, C12035, doi:10.1029/2010JC006844.

Garibotti, I. A., M. Vernet, W. A. Kozlowski, and M. E. Ferrario (2003), Composition and biomass of phytoplankton assemblages in coastal Antarctic waters: A comparison of chemotaxonomic and microscopic analyses, *Mar. Ecol. Prog. Ser.*, *247*, 27–42.

Garibotti, I. A., M. Vernet, R. C. Smith, and M. E. Ferrario (2005), Interannual variability in the distribution of the phytoplankton standing stock across the seasonal sea-ice zone west of the Antarctic Peninsula, *J. Plankton Res.*, *27*(8), 825–843.

Hall, A., and M. Visbeck (2002), Synchronous variability in the southern hemisphere atmosphere, sea ice, and ocean resulting from the annular mode, *J. Clim.*, *15*(21), 3043–3057.

Hauri, C., S. C. Doney, T. Takahashi, M. Erickson, G. Jiang, and H. W. Ducklow (2015), Two decades of inorganic carbon dynamics along the West Antarctic Peninsula, *Biogeosciences*, *12*, 6761–6779, doi:10.5194/bg-12-6761-2015.

Kang, S. H., J. S. Kang, S. Lee, K. H. Chung, D. Kim, and M. G. Park (2001), Antarctic phytoplankton assemblages in the marginal ice zone of the northwestern Weddell Sea, *J. Plankton Res.*, *23*(4), 333–352.

Kaplan, A., Y. Kushnir, M. A. Cane, and M. Benno Blumenthal (1997), Reduced space optimal analysis for historical data sets: 136 years of Atlantic sea surface temperatures, *J. Geophys. Res.*, *102*, 27,835–27,860, doi:10.1029/97JC01734.

Katz, R. W., and B. G. Brown (1991), The problem of multiplicity in research on teleconnections, *Int. J. Climatol.*, *11*, 505–513.

Knox, G. A. (2006), *Biology of the Southern Ocean*, 2nd ed., CRC Press, Boca Raton, Fla.

Kozlowski, W. A. (2008), Pigment derived phytoplankton composition along the Western Antarctic Peninsula, MS thesis, San Diego State Univ., Calif.

Liu, J., J. A. Curry, and D. G. Martinson (2004), Interpretation of recent Antarctic sea ice variability, *Geophys. Res. Lett.*, *31*, L02205, doi:10.1029/2003GL018732.

Marshall, G. J., P. A. Stott, J. Turner, W. M. Connolley, J. C. King, and T. A. Lachlan-Cope (2004), Causes of exceptional atmospheric circulation changes in the Southern Hemisphere, *Geophys. Res. Lett.*, *31*, L14205, doi:10.1029/2004GL019952.

Martinson, D. G., and R. A. Iannuzzi (1998), *Antarctic Sea Ice: Physical Processes, Interactions and Variability*, *Antart. Res. Ser.*, vol. 74, pp. 243–271, AGU, Washington, D. C.

Martinson, D. G., S. E. Stammerjohn, R. A. Iannuzzi, R. C. Smith, and M. Vernet (2008), Western Antarctic Peninsula physical oceanography and spatio–temporal variability, *Deep Sea Res., Part II*, *55*(18), 1964–1987.

McClintock, J., H. Ducklow, and W. Fraser (2008), Ecological responses to climate change on the Antarctic Peninsula, *Am. Sci.*, *96*(4), 302–310.

Meredith, M. P., M. A. Brandon, M. I. Wallace, A. Clarke, M. J. Leng, I. A. Renfrew, N. P.M. van Lipzig, and J. C. King (2008), Variability in the freshwater balance of northern Marguerite Bay, Antarctic Peninsula: Results from δ 18 O, *Deep Sea Res., Part II: Topical Studies in Oceanography*, *55*, 309–322, doi:10.1016/j.dsr2.2007.11.005.

Meredith, M. P., H. J. Venables, A. Clarke, H. W. Ducklow, M. Erickson, M. J. Leng, J. T. M. Lenaerts, and M. R. van den Broeke (2013), The freshwater system west of the Antarctic Peninsula: Spatial and temporal changes, *J. Clim.*, *26*(5), 1669–1684.

Mitchell, B. G., E. A. Brody, O. Holm-Hansen, C. McClain, and J. Bishop (1991), Light limitation of phytoplankton biomass and macronutrient utilization in the Southern Ocean, *Limnol. Oceanogr.*, *36*, 1662–1677.

Moline, M. A., and B. B. Prezelin (1996), Palmer LTER 1991–1994: Long-term monitoring and analyses of physical factors regulating variability in coastal Antarctic phytoplankton biomass, in situ productivity and taxonomic composition over subseasonal, seasonal and interannual time scales phytoplankton dynamics, *Mar. Ecol. Prog. Ser.*, *145*(1–3), 143–160.

Moline, M. A., H. Claustre, T. K. Frazer, J. Grzymskj, O. Schofield, and M. Verne (2001), Changes in phytoplankton assemblages along the Antarctic Peninsula and potential implications for the Antarctic food web.

Moline, M. A., N. J. Karnovsky, Z. Brown, G. J. Divoky, T. K. Frazer, C. A. Jacoby, J. J. Torres, and W. R. Fraser (2008), High latitude changes in ice dynamics and their impact on polar marine ecosystems, *Ann. N. Y. Acad. Sci.*, *1134*(1), 267–319.

Montes-Hugo, M., S. C. Doney, H. W. Ducklow, W. Fraser, D. Martinson, S. E. Stammerjohn, and O. Schofield (2009), Recent changes in phytoplankton communities associated with rapid regional climate change along the western Antarctic Peninsula, *Science*, *323*(5920), 1470–1473.

O'Brien, R. M. (2007), A caution regarding rules of thumb for variance inflation factors, *Qual. Quant.*, *41*, 673–690.

Parkinson, C. L. (2004), Southern Ocean sea ice and its wider linkages: Insights revealed from models and observations, *Antarct. Sci.*, *16*(4), 387–400.

Parsons, R. T., Y. Maita, and C. M. Lalli (1984), *A Manual of Chemical and Biological Methods of Seawater Analysis*, Pergammon Press, Toronto, Canada.

Pedulli, M., J. J. Bisagni, H. W. Ducklow, R. Beardsley, and C. Pilskaln (2014), Estimates of potential new production (PNP) for the waters off the western Antarctic Peninsula (WAP) region, *Cont. Shelf Res.*, *84*, 54–69.

Prézelin, B. B., E. E. Hofmann, C. Mengelt, and J. M. Klinck (2000), The linkage between Upper Circumpolar Deep Water (UCDW) and phytoplankton assemblages on the west Antarctic Peninsula continental shelf, *J. Mar. Res.*, *58*(2), 165–202.

Ross, R. M., L. B. Quetin, D. G. Martinson, R. A. Iannuzzi, S. E. Stammerjohn, and R. C. Smith (2008), Palmer LTER: Patterns of distribution of five dominant zooplankton species in the epipelagic zone west of the Antarctic Peninsula, 1993–2004, *Deep Sea Res., Part II*, *55*(18), 2086–2105.

Rubin, S. I., T. Takahashi, D. W. Chipman, and J. G. Goddard (1998), Primary productivity and nutrient utilization ratios in the Pacific sector of the Southern Ocean based on seasonal changes in seawater chemistry, *Deep Sea Res., Part I*, *45*, 1211–1234.

Rysgaard, S., J. Mortensen, T. Juul-Pedersen, L. L. Sørensen, K. Lennert, D. H. Søgaard, K. E. Arendt, M. E. Blicher, M. K. Sejr, and J. Bendtsen (2012), High air-sea CO_2 uptake rates in nearshore and shelf areas of Southern Greenland: Temporal and spatial variability, *Mar. Chem.*, *128–129*, 26–33.

Saba, G. K., et al. (2014), Winter and spring controls on the summer food web of the coastal West Antarctic Peninsula, *Nat. Commun.*, *5*, 4318.

Schloss, I. R., D. Abele, S. Moreau, S. Demers, A. Valeria Bers, O. González, and G. A. Ferreyra (2012), Response of phytoplankton dynamics to 19–year (1991–2009) climate trends in Potter Cove (Antarctica), *J. Mar. Syst.*, *92*(1), 53–66.

Schofield, O., H. W. Ducklow, D. G. Martinson, M. P. Meredith, M. A. Moline, and W. R. Fraser (2010), How do polar marine ecosystems respond to rapid climate change? *Science*, *328*(5985), 1520–1523.

Serebrennikova, Y., K. A. Fanning, and J. J. Walsh (2008), Modeling the nitrogen and carbon cycling in Marguerite Bay, Antarctica: Annual variations in ammonium and net community production, *Deep Sea Res., Part II*, *55*(3), 393–411.

Serebrennikova, Y. M., and K. A. Fanning (2004), Nutrients in the Southern Ocean GLOBEC region: Variations, water circulation, and cycling, *Deep Sea Res., Part II: Topical Studies in Oceanography*, *51*, 1981–2002, doi:10.1016/j.dsr2.2004.07.023.

Smith, R. C., S. E. Stammerjohn, and K. S. Baker (1996), Surface air temperature variations in the Western Antarctic Peninsula region, in *Foundations for Ecological Research West of the Antarctic Peninsula*, pp. 105–121, AGU, Washington, D. C.

Smith, R. C., K. S. Baker, and M. Vernet (1998), Seasonal and interannual variability of phytoplankton biomass west of the Antarctic Peninsula, *J. Mar. Syst.*, *17*(1), 229–243.

Smith, R. C., D. G. Martinson, S. E. Stammerjohn, R. A. Iannuzzi, and K. Ireson (2008), Bellingshausen and western Antarctic Peninsula region: Pigment biomass and sea-ice spatial/temporal distributions and interannual variability, *Deep Sea Res., Part II*, *55*(18), 1949–1963.

Stammerjohn, S. E., D. G. Martinson, R. C. Smith, X. Yuan, and D. Rind (2008), Trends in Antarctic annual sea ice retreat and advance and their relation to El Niño–Southern Oscillation and Southern Annular Mode variability, *J. Geophys. Res.*, *113*, C03S90,, doi:10.1029/2007JC004269.

Thomas, E. R., G. J. Marshall, and J. R. McConnell (2008), A doubling in snow accumulation in the western Antarctic Peninsula since 1850, *Geophys. Res. Lett.*, *35*, L01706, doi:10.1029/2007GL032529.

Tomczak, M., and D. G. B. Large (1989), Optimal multiparameter analysis of mixing in the thermocline of the Eastern Indian Ocean, *J. Geophys. Res.*, *94*, 16,141–16,149, doi:10.1029/JC094iC11p16141.

Trull, T. S., S. R. Rintoul, E. R. Hadfield, and E. R. Abraham (2001), Circulation and seasonal evolution of polar waters south of Australia: Implications for iron fertilisation of the Southern Ocean, *Deep Sea Res., Part II*, *48*, 2439–2466.

Vaughan, D. G., G. J. Marshall, W. M. Connolley, C. Parkinson, R. Mulvaney, D. A. Hodgson, J. C. King, C. J. Pudsey, and J. Turner (2003), Recent rapid regional climate warming on the Antarctic Peninsula, *Clim. Change*, *60*(3), 243–274.

Venables, H. J., A. Clarke, and M. P. Meredith (2013), Wintertime controls on summer stratification and productivity at the western Antarctic Peninsula, *Limnol. Oceanogr.*, *58*(3), 1035–1047.

Vernet, M., D. G. Martinson, R. A. Iannuzzi, S. Stammerjohn, W. Kozlowski, K. Sines, R. Smith, and I. Garibotti (2008), Primary production within the sea-ice zone west of the Antarctic Peninsula: I—Sea ice, summer mixed layer, and irradiance, *Deep Sea Res., Part II*, *55*(18), 2068–2085.
Villafañe, V., E. W. Helbling, and O. Holm-Hansen (1993), Phytoplankton around Elephant Island, Antarctica, *Polar Biol.*, *13*(3), 183–191.
Walsh, J. J., D. A. Dieterle, and J. Lenes (2001), A numerical analysis of carbon dynamics of the Southern Ocean phytoplankton community: The roles of light and grazing in affecting both sequestration of atmospheric CO_2 and food availability to larval krill, *Deep Sea Res., Part I*, *48*, 1–48.
Yuan, X. (2004), ENSO-related impacts on Antarctic sea ice: A synthesis of phenomenon and mechanisms, *Antarct. Sci.*, *16*(4), 415–425.
Yuan, X., and D. G. Martinson (2000), Antarctic sea ice extent variability and its global connectivity, *J. Clim.*, *13*(10), 1697–1717.